PERGAMON

International Journal of Multiphase Flow 28 (2002) 325–346

International Journal of Multiphase Flow

www.elsevier.com/locate/ijmulflow

Vortex pairing in two-way coupled, particle laden mixing layers

E. Wallner [1], E. Meiburg *

Department of Mechanical and Environmental Engineering, University of California at Santa Barbara, Santa Barbara, CA 93106, USA

Received 14 November 2000; accepted 5 November 2001

Abstract

The role of two-way interphase coupling effects in subharmonically forced, dilute, particle laden mixing layers is investigated. Temporally growing Lagrangian–Eulerian numerical simulations address both uniformly as well as differentially seeded flows. Emphasis is placed on a *vorticity*-based interpretation of the simulation results. Expanding the fluid vorticity source term due to two-way coupling demonstrates the importance of particle concentration gradients and 'slip vorticity'. For uniformly laden mixing layers and intermediate *St* particles, the reduction in the growth rate of the Kelvin–Helmholtz instability by the two-way coupling effects also slows down vortex pairing. At large *St*, a layered vorticity structure in the outer regions of the vortex cores results from the thick or even double banded nature of the braids. By causing the vortices to rotate around each other, the subharmonic forcing also enhances the particle transport away from the center of the mixing layer. Intermediate *St* particles are seen to benefit the most from this mechanism, so that they can, at least temporarily, exceed the dispersion rate of the passive case. For differentially loaded mixing layers, the vorticity source term is seen to cause an asymmetry in the pairing process, by weakening the upstream and strengthening the downstream vortex, which subsequently dominates the pairing. For intermediate *St* particles, this asymmetry leads to a more rapid ejection of particles from the downstream vortex. For large *St* particles, the braid region in between vortex pairs is seen to thicken and to roll up, thereby causing the emergence of a satellite vortex. Somewhat surprisingly, the results indicate that in a streamwise averaged sense the two-way coupling effects do not significantly alter the integral particle dispersion measure for subharmonically forced, differentially loaded mixing layers. Throughout, frequent comparisons with experimental data are made.

* Corresponding author. Tel.: +1-805-893-5278; fax: +1-805-893-5278.

E-mail address: meiburg@engineering.ucsb.edu (E. Meiburg).

[1] Present address: Institute of Flight Mechanics and Flight Control, University of Stuttgart, Pfaffenwaldring 7a, D-70550 Stuttgart, Germany.

0301-9322/02/$ - see front matter
PII: S0301-9322(01)00083-0

1. Introduction

In recent years, experimental as well as numerical and theoretical investigations have been able to reveal several important aspects of the two-way coupling mechanisms that dominate dilute, particle laden flows. Their effects on the statistical properties of both isotropic and homogeneous turbulence have been addressed in the numerical simulations of several authors (Squires and Eaton, 1990; Elghobashi and Truesdell, 1993; Truesdell and Elghobashi, 1994; Maxey et al., 1997; Sundaram and Collins, 1999), while other investigators have focused on the modification of wall turbulence (Pan and Banerjee, 1996), fully developed channel flows (Kulick et al., 1994), and separated flows (Fessler and Eaton, 1999) by heavy particles. Wallner and Meiburg (1998) and Meiburg et al. (2000) have addressed the effects of particle loading on the nonlinear stages of fundamentally forced, transitional free shear flows by means of Lagrangian–Eulerian simulations. They present a vorticity based interpretation of the two-way coupling effects and show that these are related to the misalignment of the concentration gradient and the slip velocity, as well as to the difference in fluid and particle vorticities. For uniformly seeded mixing layers, their simulations confirm some of the features observed by Druzhinin (1995) for the model problem of a two-way coupled, particle laden Stuart vortex, as well as by Dimas and Kiger (1998) in a linear stability analysis. For small values of the Stokes number, a mild destabilization of the mixing layer is observed. At moderate and large Stokes numbers, on the other hand, the transport of vorticity from the braids into the core of the evolving Kelvin–Helmholtz vortices is seen to be slowed by the two-way coupling effects. As a result, the particle ejection from the vortex cores is weakened. For constant mass loadings, the two-way coupling effects are strongest at intermediate Stokes number values. Moderately large Stokes numbers result in the formation of two bands of high particle concentration in the braids. For mixing layers in which only one stream is seeded, the particle concentration gradient across the mixing layer leads to strong vorticity production and loss, which results in an effective net motion of the vortex in the flow direction of the seeded stream.

While our earlier work focused on two-way coupling effects in the presence of fundamental forcing only, the present investigation addresses the subject of vortex pairing in particle laden mixing layers, which is known to dominate the growth of the flow in the streamwise direction (Winant and Browand, 1974). This topic is also at the heart of the experimental work by Kiger and Lasheras (1995), who analyze the kinetic energy transfer between the two phases in a droplet laden mixing layer, cf. also Kiger and Lasheras (1997). For a differentially laden mixing layer, these authors observe the vortex pairing mechanism to play a homogenizing role with respect to the overall particle dispersion. However, at the same time they demonstrate a clear distinction between the effects of the vortex pairing mechanism on small and large particles, respectively. Small particles, i.e., those with a Stokes number much less than unity, are well mixed, while particles with a Stokes number of order unity or larger still display mostly inhomogeneous dispersion. Throughout the present investigation, the importance of the fluid vorticity variable, and of the ways in which it is affected by the two-way coupling, will be emphasized, in order to develop a vorticity-based interpretation of the two-way coupling mechanisms in free shear flows.

The paper is organized as follows: Section 2 states the governing equations and derives the relevant dimensionless parameters. Subsequently, Section 3 briefly describes the combined Lagrangian–Eulerian numerical approach. In Section 4 results are presented for both uniformly

and differentially loaded, subharmonically perturbed mixing layers. Finally, Section 5 will present a brief summary and discussion of the results.

2. Governing equations

2.1. Two-way coupling via the momentum equation

Following earlier authors, e.g., Squires and Eaton (1990), Elghobashi and Truesdell (1993), Maxey et al. (1997), Wallner and Meiburg (1998), Meiburg et al. (2000), we account for the momentum coupling between particle and fluid motion by assuming that each particle locally exerts a force on the fluid that is opposite and equal to the force experienced by the particle, cf. Williams (1985). In order to determine the collective force density $\vec{l}$ with which the particles located in a differential control volume act on the fluid, one defines the average particle velocity $\vec{\bar{u}}_{\mathrm{p}}(\vec{x},t)$ in the differential control volume. Assuming a Stokes drag force, one thus obtains the dimensional relationship

$$\vec{l} = n3\pi\mu d_{\mathrm{p}}(\vec{\bar{u}}_{\mathrm{p}} - \vec{u}), \tag{1}$$

where n is the particle number density, μ denotes the fluid viscosity, d_{p} is the particle diameter, and $\vec{u}$ indicates the fluid velocity. In focusing on the coupling mechanisms of dilute particle or droplet laden flows, we neglect the volume fraction of the particle phase in the continuity equation for the fluid. This approximation is valid when investigating, for example, the dynamics of sprays or aerosols, where for typical mass loadings of O(1) the volume fraction of the particulate phase is of $O(10^{-3})$. Note that we use 'particles' and 'spray' interchangeably here, as we do not distinguish between solid particles and droplets. Furthermore, interactions among the particles as well as such effects as evaporation and atomization are not considered here.

The mass and momentum equations governing the constant density fluid motion thus take the form

$$\nabla \cdot \vec{u} = 0, \tag{2a}$$

$$\rho\frac{\partial \vec{u}}{\partial t} + \rho(\vec{u}\cdot\nabla)\vec{u} = -\nabla p + \mu\nabla^2\vec{u} + n3\pi\mu d_{\mathrm{p}}\ (\vec{\bar{u}}_{\mathrm{p}} - \vec{u}). \tag{2b}$$

Upon non-dimensionalization, we obtain

$$\nabla \cdot \vec{u} = 0, \tag{3a}$$

$$\frac{\partial \vec{u}}{\partial t} + (\vec{u}\cdot\nabla)\vec{u} = -\nabla p + \frac{1}{Re}\nabla^2\vec{u} + n\frac{D}{St}(\vec{\bar{u}}_{\mathrm{p}} - \vec{u}). \tag{3b}$$

Here the Reynolds number Re, the dimensionless mass loading D, and the particle Stokes number St, respectively, are defined as

$$Re = \frac{UL}{\nu}, \quad D = \frac{\bar{\rho}_{\mathrm{p}}}{\rho}, \quad St = \frac{d_{\mathrm{p}}^2\rho_{\mathrm{p}}U}{18\mu L}, \tag{4}$$

where

$$\bar{\rho}_{\mathrm{p}} = m_{\mathrm{p}} N \tag{5}$$

denotes the nominal mass of particle material per unit volume of the flow in the seeded stream. U and L represent the velocity difference and width across the mixing layer, respectively.

For the case of particles that are much smaller than the characteristic length scales of the velocity field, an equation of motion was formulated by Maxey and Riley (1983). Since our interest focuses on situations in which the density of the particle material is much greater than that of the fluid, several of the terms in that equation become negligible, cf. the order of magnitude analysis conducted by Lazaro and Lasheras (1989). By furthermore assuming Stokes flow around the particles, we obtain

$$\frac{\mathrm{d}\vec{u}_{\mathrm{p}}}{\mathrm{d}t} = \frac{3\pi\mu d_{\mathrm{p}}}{m_{\mathrm{p}}}\left[\vec{u}(\vec{x}_{\mathrm{p}}) - \vec{u}_{\mathrm{p}}\right]. \tag{6}$$

This equation expresses the balance of particle inertia and viscous drag only.

We aim at identifying the mechanisms by which the two-way coupling effects can alter the vorticity dynamics of single phase free shear flows, similar in spirit to the linear stability investigation of Dimas and Kiger (1998). Hence it is instructive to formulate the conservation equations for the fluid motion in terms of the vorticity variable ω, cf. Druzhinin (1995). For the present situation of two-dimensional flows, we employ a formulation based on the streamfunction ψ, which results in

$$\frac{\partial\omega}{\partial t} + (\vec{u}\cdot\nabla)\omega = \frac{1}{Re}\nabla^2\omega + \frac{D}{St}\nabla\times\left[n(\vec{u}_{\mathrm{p}} - \vec{u})\right]\cdot\vec{e}_z, \tag{7a}$$

$$\nabla^2\psi = -\omega, \tag{7b}$$

$$u = \frac{\partial\psi}{\partial y}, \tag{7c}$$

$$v = -\frac{\partial\psi}{\partial x}. \tag{7d}$$

We note that both spatial variations in the particle number density field, as well as local velocity differences (slip velocities) between the two phases can lead to the production or cancellation of vorticity. For a more detailed discussion and interpretation of the vorticity source term, cf. below.

3. Numerical approach for the two-dimensional problem

The investigation focuses on the evolution of the base flow

$$\vec{u}(y, t=0) = (0.5\tanh y, 0)^{\mathrm{T}} \tag{8}$$

in the presence of both a basic and a subharmonic perturbation. In order to avoid the high costs of performing a simulation of the so-called spray equation (Williams, 1985) for the particle concentration distribution in the higher-dimensional phase space, we follow other authors (Squires and Eaton, 1990; Elghobashi and Truesdell, 1993; Truesdell and Elghobashi, 1994; Kulick et al., 1994; Fessler and Eaton, 1999) and pursue a less expensive Lagrangian numerical

method for the particulate phase, which is coupled to an Eulerian treatment of the fluid, cf. Wallner and Meiburg (1998) and Meiburg et al. (2000). Its features will be outlined in the following.

The field equations (7a) and (7b) for the fluid phase are solved in an Eulerian fashion, by applying a spectral Fourier series expansion in the streamwise, periodic direction (Gottlieb and Orszag, 1977), and sixth-order compact finite differences in the transverse direction (Lele, 1992). Time advancement is accomplished by means of a third-order Runge–Kutta method (Wray, 1991). An initial perturbation is applied to the fluid velocity field that has the form of the eigenfunction of the most unstable mode according to inviscid linear stability theory as found by Michalke (1964). Its wavenumber is $\alpha = 0.4446$ for the fundamental mode. The length of the computational domain is chosen such that it accommodates exactly two wavelengths of the fundamental perturbation. Its vertical size slightly exceeds its horizontal extent, so that the boundaries are sufficiently far away from the mixing layer to prevent them from influencing the flow in any significant manner. Both the fundamental and the subharmonic perturbations initially have an amplitude of 0.005. Throughout the investigation, the value of *Re* is taken to be 200. Slip conditions are applied at the upper and lower boundaries of the control volume. The simulations typically employ a discretization of 65 points per subharmonic wavelength. The size of the time step strongly depends on the magnitude of the dimensionless parameters, as they effectively control the range of convection velocities and diffusive/dispersive effects. At the beginning of the simulation, the particle velocities are set equal to the local fluid velocity.

Our numerical approach for modeling the particulate phase and its effects on the fluid motion builds on the physical principles reviewed by Williams (1985), and it is similar in its Lagrangian nature to the techniques employed by Squires and Eaton (1990), Elghobashi and Truesdell (1993) and Maxey et al. (1997) in that it tracks individual particles with inertia in a Lagrangian fashion. However, while those authors focused on the two-way coupling mechanisms between the particulate phase and a turbulent carrier flow in a velocity–pressure formulation of the equations governing the fluid motion, the simulations to be discussed in the following will be based on the vorticity formulation (7a) and (7b) of the governing equations.

The dispersed particles are tracked in a Lagrangian way, with each of the N computational particles representing a cluster of physical particles located in the same neighborhood. Each cluster moves as a single virtual particle. The number density field $n(\vec{x}, t)$ is then obtained as

$$n(\vec{x}, t) = \sum_{i=1}^{N} \Gamma_i \gamma_i [\vec{x} - \vec{x}_i(t)]. \tag{9}$$

Here γ_i represents the generic shape function of the number density distribution within computational particle i, normalized so that

$$\int \gamma_i(\vec{x})\, \mathrm{d}\vec{x} = 1. \tag{10}$$

In the present investigation, we take γ_i to be radially symmetric and of Gaussian shape

$$\gamma_i(r) = \frac{1}{\pi \sigma_i^2} \mathrm{e}^{-r^2/\sigma_i^2}, \tag{11}$$

where σ_i is a measure of the core size of the computational cluster. Γ_i denotes the 'strength' of cluster i, i.e., the overall number of physical particles contained in it. If at time $t = 0$ the clusters are separated by a distance Δ in the x- and y-directions, we obtain

$$\Gamma_i = \Delta^2 n(\vec{x}_i, 0). \tag{12}$$

In the numerical simulations to be discussed below, all computational clusters initially are of identical size and strength. Their initial separation Δ is typically equal to the grid size of the Eulerian mesh, while their core size $\sigma = 2\Delta$. In this way, there is sufficient overlap between the particle clusters to ensure a smooth number density field. In order to maintain a well-resolved particle concentration field for long times, a remeshing procedure for the particles is employed which inserts an additional cluster if the distance between two initially neighboring clusters exceeds a certain value. The strengths Γ_i of the two original clusters and the new, additional cluster are then adjusted in order to maintain the overall number of particles in the flowfield. Within the present study, we follow the relatively simple rule that if the original neighbors had strengths Γ_1^* and Γ_2^* before the remeshing, their new strengths are determined as $\Gamma_1 = \frac{3}{4}\Gamma_1^*$ and $\Gamma_2 = \frac{3}{4}\Gamma_2^*$. The new cluster, which is introduced halfway between the original ones, and with their average velocity, is given the strength $\Gamma_3 = \frac{1}{4}(\Gamma_1^* + \Gamma_2^*)$.

In order to evaluate the instantaneous acceleration of each Lagrangian cluster, the flow velocity at its location is determined by means of a fourth-order, two-dimensional Lagrangian interpolation scheme (Martin and Meiburg, 1994). The particle velocity is taken as a weighted average of the cluster velocities. It should be noted that this approach is valid only for a linear drag law, whereas a more complicated drag law would require a different averaging procedure. Clusters that leave the control volume in the horizontal x-direction are reintroduced at the opposite boundary, in accordance with the periodic boundary conditions in the streamwise direction.

An important point concerns the streamfunction boundary conditions at the top and bottom of the computational domain. For the corresponding single-phase problem, if the initial conditions and symmetry properties are such that there is no net mass flux in the horizontal x-direction, one can specify $\psi = 0$ at these boundaries for all times. For the two-way coupled two-phase problem, on the other hand, this boundary condition will hold only if the initial conditions as well as the dynamical equations for the particulate phase satisfy corresponding symmetry properties. This will not be the case if, for example, only one of the two streams is seeded, or if gravity forces act on the particles. Under such conditions, there can be a net x-momentum transfer from the particles to the fluid, which will cause an overall acceleration of the fluid in the streamwise direction. Within our inertial reference frame, this will result in the generation of a potential component U_{pot} of the fluid velocity in the x-direction, which can be obtained as

$$\frac{\mathrm{d}U_{\mathrm{pot}}}{\mathrm{d}t} = \frac{D}{St}\bar{s}_x, \tag{13}$$

where $\bar{s}_x$ denotes the x-component of the momentum source term, averaged over the entire flowfield. Regarding the validation of the numerical approach, cf. Wallner and Meiburg (1998) as well as Meiburg et al. (2000).

4. Results of two-dimensional simulations for subharmonically perturbed mixing layers

Key to understanding the two-way coupling mechanisms is the fluid vorticity equation (7a). Upon expanding

$$\nabla \times \left[n(\vec{u}_p - \vec{u}) \right] = \nabla n \times (\vec{u}_p - \vec{u}) + n\left(\nabla \times \vec{u}_p - \nabla \times \vec{u} \right), \tag{14}$$

two potential mechanisms for the generation or cancellation of vorticity are identified. The first term indicates that the vorticity will be altered if the concentration gradient is misaligned with the direction of the slip velocity. The second term describes the influence of a difference between the particle and fluid vorticities. A mixing layer in which only one of the streams contains particles, such as in the flow investigated by Kiger and Lasheras (1995), will at least initially be dominated by the first term, due to the strong particle concentration gradients that exist when the streams first come together. It is much less clear how dominant this term will be at later times, when the well-known emergence of particle streaks or 'tongues' leads to much more convoluted regions of

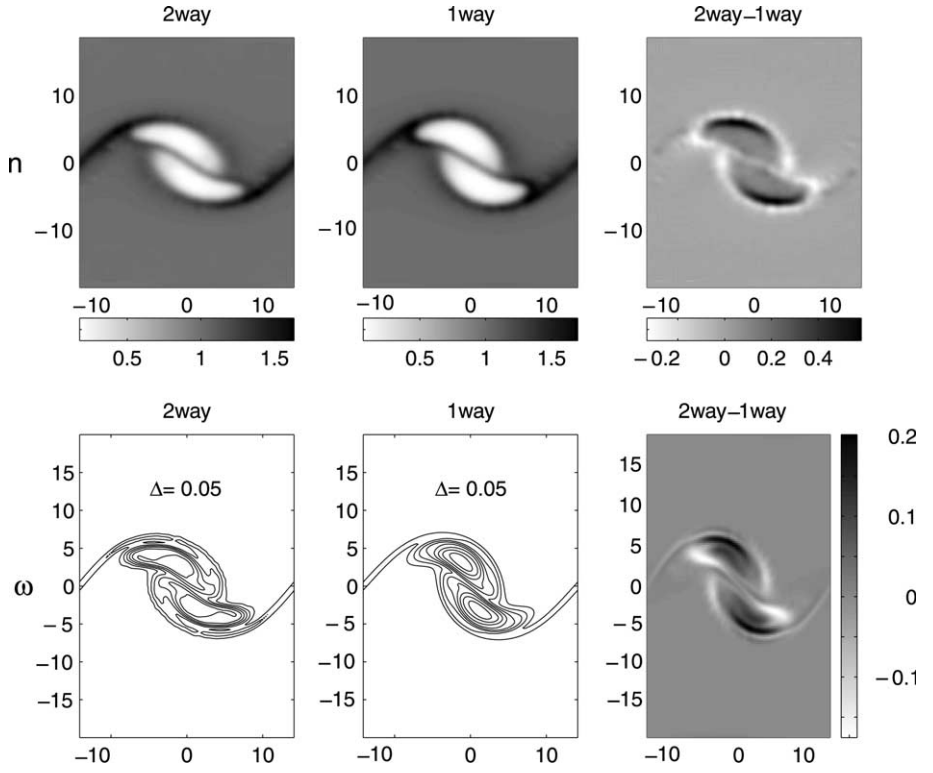

Fig. 1. $St = 1$, $D = 0.5$, $Re = 200$, $t = 37.5$: Particle concentration and fluid vorticity fields for coupled and passive cases. In the vorticity contour plots, Δ gives the increment between contour levels. The difference in vorticity is shown by shading, where light shading visualizes an increase, and dark shading a decrease in the vorticity magnitude due to coupling. In the two-way coupled case, more vorticity can still be found in the braids between the pairing vortices, while the vortex cores remain somewhat weaker.

steep concentration gradients, which in turn can result in geometrically complex or layered distributions of the vorticity source term.

For mixing layers uniformly laden with particles, a very different situation presents itself. Our earlier simulations (Meiburg et al., 2000), which contained a fundamental perturbation only, show that under these circumstances in the vicinity of the core the second term initially is largest. This is due to the particles' inertia, which locally can result in the emergence of a substantial 'slip vorticity' of the particles that tends to reduce the magnitude of the fluid vorticity. Keeping in mind that, for the present initial conditions, the fluid vorticity is negative everywhere, the source term thus is positive. In the braids, on the other hand, the first term on the right-hand side of Eq. (14) may become more significant again due to the large variations of the particle concentration field, and the relatively weak vorticity of the fluid. In the absence of subharmonic perturbations, the local configuration in the stagnation point region between the rollers thus leads to a quadrupole structure of the vorticity source term.

In the present investigation, the focus is on two-way coupling mechanisms in mixing layers subject to subharmonic vortex pairing events, which were shown by Winant and Browand (1974) to be the dominant mechanism in mixing layer growth. One of the goals is to evaluate how the above, initially dominant dynamical mechanisms persist in the presence of vortex pairing triggered by subharmonic forcing. The simulations to be presented in the following are characterized

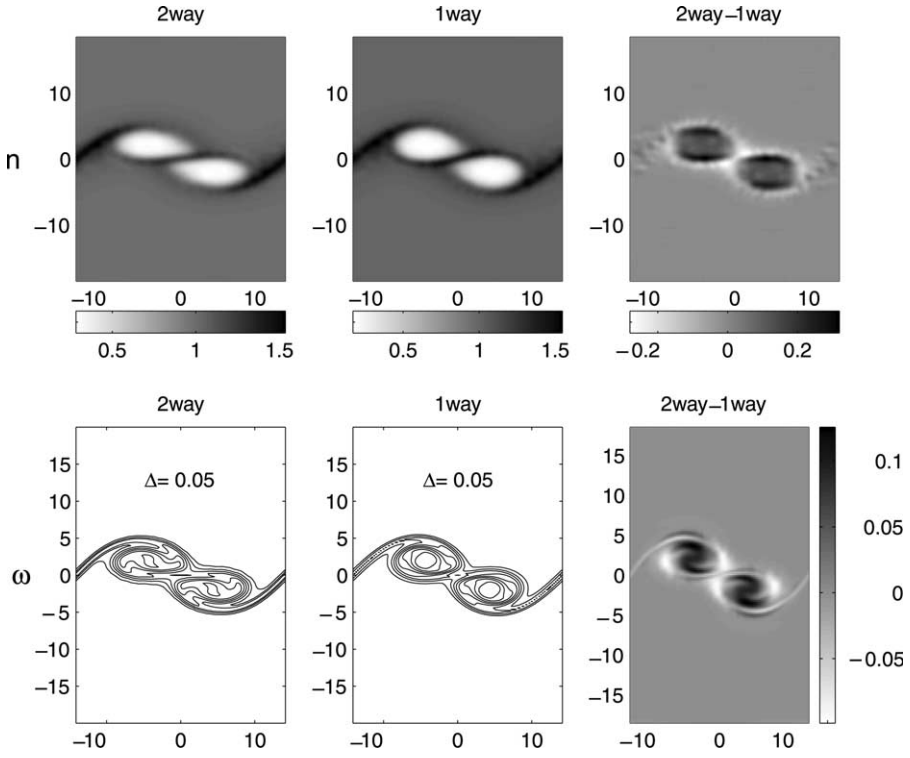

Fig. 2. $St = 1$, $D = 0.5$, $Re = 200$, $t = 50$: Particle concentration and fluid vorticity fields for coupled and passive cases. The pairing process proceeds somewhat more slowly in the two-way coupled case.

by equal initial amplitudes of the fundamental and subharmonic perturbations. Furthermore, the initial phase of the subharmonic is chosen to have a maximum in between the two evolving vortices, which is the most amplified configuration.

4.1. Uniform particle loading

In this case the initial concentration field is uniform, so that the first term on the right-hand side of Eq. (14) will not play a dominant role during the early flow stages. Fig. 1 shows a plot that compares the passive and coupled cases for an intermediate Stokes number of unity, a moderate mass loading ratio $D = 0.5$, and $Re = 200$ at the early time of 37.5, while Fig. 2 depicts the later time $t = 50$. We recognize several interesting features of the two-way coupled flow that reflect the vorticity mechanisms outlined in our preliminary discussion of Eq. (14) above. The magnitude of the vorticity in the cores is somewhat reduced compared to the passive case. This indicates the influence of the slip vorticity term, and it results in an overall slower accumulation of vorticity in the vortex cores. The transport of vorticity from the braids into the cores, i.e., the growth of the

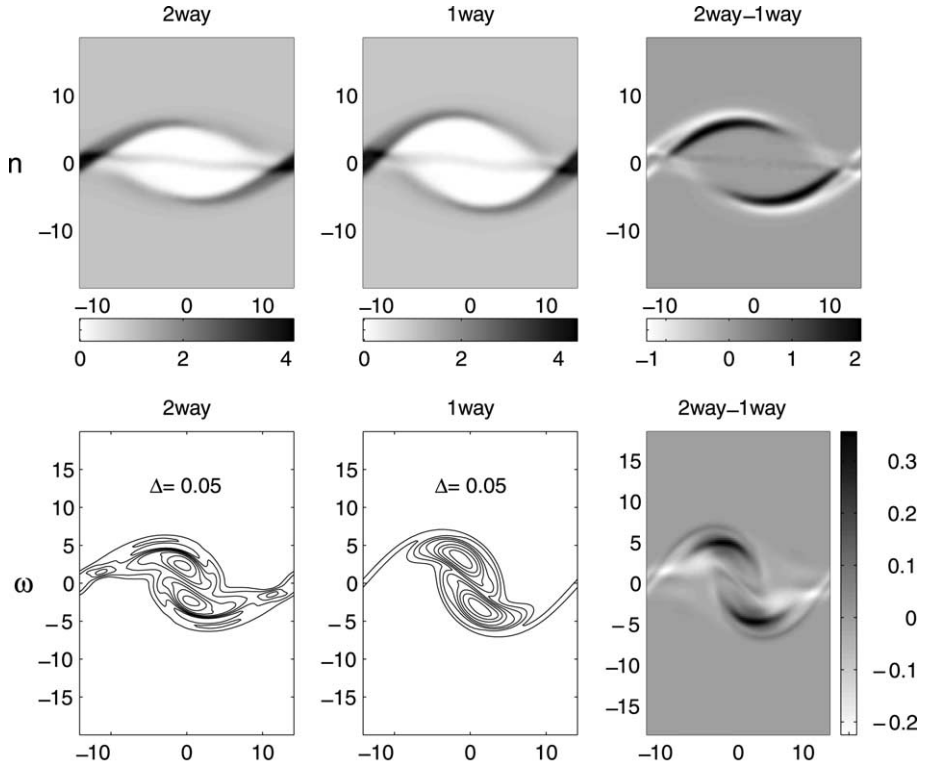

Fig. 3. $St = 10$, $D = 0.5$, $Re = 200$, $t = 37.5$: Particle concentration and fluid vorticity fields for coupled and passive cases. Two-way coupling results in substantially thicker braids, both in between pairing vortices, as well as in between vortex pairs.

Kelvin–Helmholtz instability, thus is effectively slowed down, which in turn means that the particle ejection from the vortex cores proceeds at a reduced rate in the two-way coupled case.

Similarly to the passive case, the two-way coupled case exhibits concentrated particle bands in the braid region. These bands represent thin layers of high particle concentration embedded in a large region of nearly uniform concentration. According to the first term on the right-hand side of Eq. (14), this configuration results in thin, opposite-signed vorticity source layers along the edges of the particle band. Through a combination of vorticity production and cancellation, these vorticity source layers will effectively shift the original thin braid vorticity layer in the transverse direction. Interestingly, the braid between the pairing vortices is depleted of particles much more rapidly than the braid in between two vortex pairs, so that the above mechanisms affect the two braid regions to different degrees. This difference is not present in flows that are forced by a fundamental frequency only. Fig. 1 clearly shows that the braid in between the pairing vortices thickens as a result of the above two-way coupling effects. These observations regarding the influence of the subharmonic perturbation are in agreement with some of the experimental findings of Kiger and Lasheras (1995), even though their work addresses mixing layers with only one particle laden stream. In the 'transition region', where the subharmonic perturbation exhibits

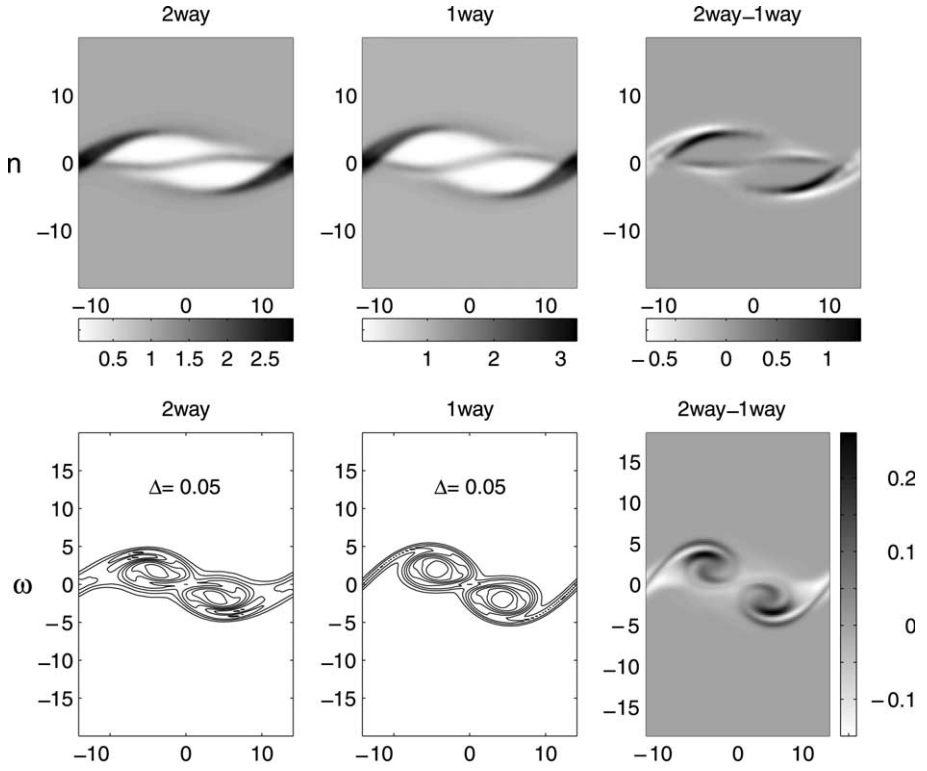

Fig. 4. $St = 10$, $D = 0.5$, $Re = 200$, $t = 50$: Particle concentration and fluid vorticity fields for coupled and passive cases. The particle ejection from the vortices is not as pronounced, so that the particle concentration distribution remains more flattened.

strong growth, these authors find the streaks between pairing vortices to be weaker than those in between vortex pairs. The particles contained in these weaker streaks subsequently are rapidly dispersed into the subharmonic structure, so that effectively only the streak in between the paired vortices remains.

It is well established that the vortex pairing mechanism itself feeds on the fundamental Kelvin–Helmholtz instability. Thus it is not surprising that the slower growth of the Kelvin–Helmholtz instability in the two-way coupled case results in a slowdown of the pairing as well. This can be recognized in Fig. 2, which indicates a slightly slower rotation of the vortex cores around each other in the two-way coupled case.

For particles of $St = 10$, two-way coupling affects the flow field in a much more pronounced fashion, cf. Figs. 3 and 4. As compared to the one-way coupled case, both of the braid regions are now substantially thicker. This is due to the added inertia of the particles, which enables them to overshoot the stagnation point region, so that much thicker bands or even two distinct bands of high particle concentration can form, especially in the braid between two vortex pairs, cf. also the passive case analyzed by Martin and Meiburg (1994). An additional effect of the increased particle inertia is that more particles remain in the braid region between the pairing vortices for longer times. Just as for the smaller particles, the growth of the Kelvin–Helmholtz instabilty, and thereby of the vortex pairing process, is slowed down somewhat by the two-way coupling. Consequently, the particle ejection is not as pronounced in the two-way coupled case, so that the particle concentration field appears much more flattened than in the passive case. This is again in agreement

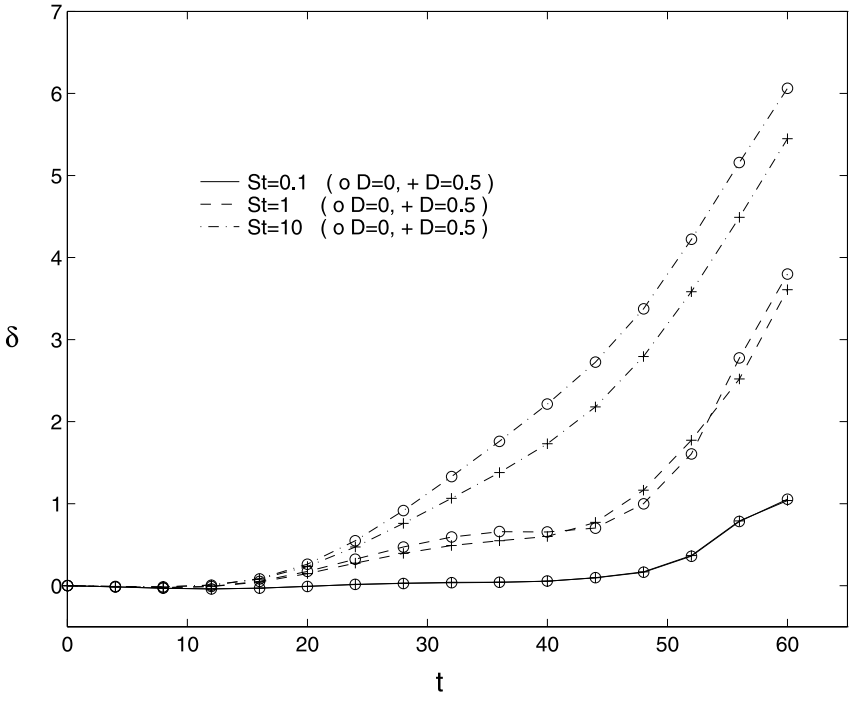

Fig. 5. Influence of St and two-way coupling on the weighted particle dispersion thickness for subharmonically perturbed, uniformly seeded flow.

with the observations of Kiger and Lasheras (1995), who find that heavier particles cannot be ejected into the opposite stream as easily as smaller particles.

The vorticity field clearly reflects these two-way coupling effects. Not only is the vorticity magnitude in the vortex cores reduced due to the slip vorticity, but additional layered vorticity structures appear in the outer regions of the vortex cores. These vorticity layers reflect the action of the concentration gradient term in Eq. (14) in response to the bands of high particle concentration. The additional fine scale vorticity thus generated within the vortex cores can potentially lead to a more rapid transition to turbulence, as well as to increased mixing of fluid and particles.

In order to quantify the particle displacement process, we follow Martin and Meiburg (1994) and define the weighted particle displacement thickness

$$\delta(t) = \frac{1}{L}\int_{-L/2}^{L/2}\int_{-\infty}^{0} |y|(n(x,y,t) - n_\infty)\,\mathrm{d}y\,\mathrm{d}x. \tag{15}$$

Fig. 5 shows the growth of δ over time for $St = 0.1$, 1, and 10, for subharmonically perturbed mixing layers with and without two-way coupling effects. Overall, the $St = 10$ particles are dispersed most efficiently, regardless of whether or not two-way coupling effects are included. The dispersion of these relatively heavy particles clearly deteriorates when two-way coupling effects are considered, due to the overall damping of the mixing layer instability by the dispersed phase. This quantitative finding is in agreement with the 'flattening' of the particle concentration contours visible in Fig. 4.

Particles of $St = 1$ display a qualitatively different behavior. For short times, their dispersion deteriorates as a result of the two-way coupling effects, in line with our findings for fundamentally

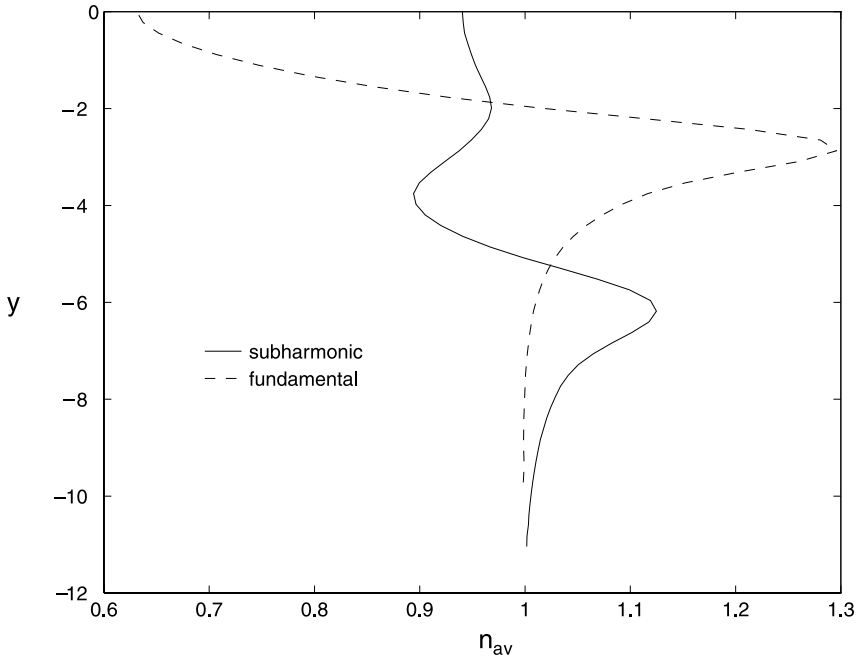

Fig. 6. Streamwise averaged particle concentration profile for $St = 1$, $D = 0.5$, $Re = 200$, and $t = 50$. The vortex pairing instability effectively homogenizes the particle concentration field.

perturbed two-way coupled mixing layers (Meiburg et al., 2000). For intermediate times however, i.e., as the subharmonic perturbation grows in importance, dispersion in the coupled case begins to exceed that of the passive case. This reflects the fact that the dispersion is no longer caused exclusively by ejection from the vortex core. In addition, the large scale rotational fluid motion associated with the vortex pairing process now contributes to the transport of the particles away from the mixing layer centerline. In this regard, it appears to be advantageous that more particles remain in the vortex centers for longer times in the two-way coupled case, as they can benefit from the large scale motion of these vortices. Eventually, however, the damping effects win out, and the displacement thickness for the passive case once again outgrows its two-way coupled counterpart.

For the $St = 0.1$ particles, the two-way coupling mechanisms are seen to have a negligible effect on the weighted particle displacement thickness. This reflects the fact that the particles follow the fluid motion quite faithfully, without altering it substantially.

The reason for the higher weighted particle displacement thickness values in the subharmonically forced case as compared to the fundamental case can be understood on the basis of the streamwise averaged concentration profiles shown in Fig. 6. This plot corresponds to a time when the pairing has already largely taken place. In the subharmonic case we find a much more homogeneous concentration profile than in the fundamental counterpart. This is in agreement with

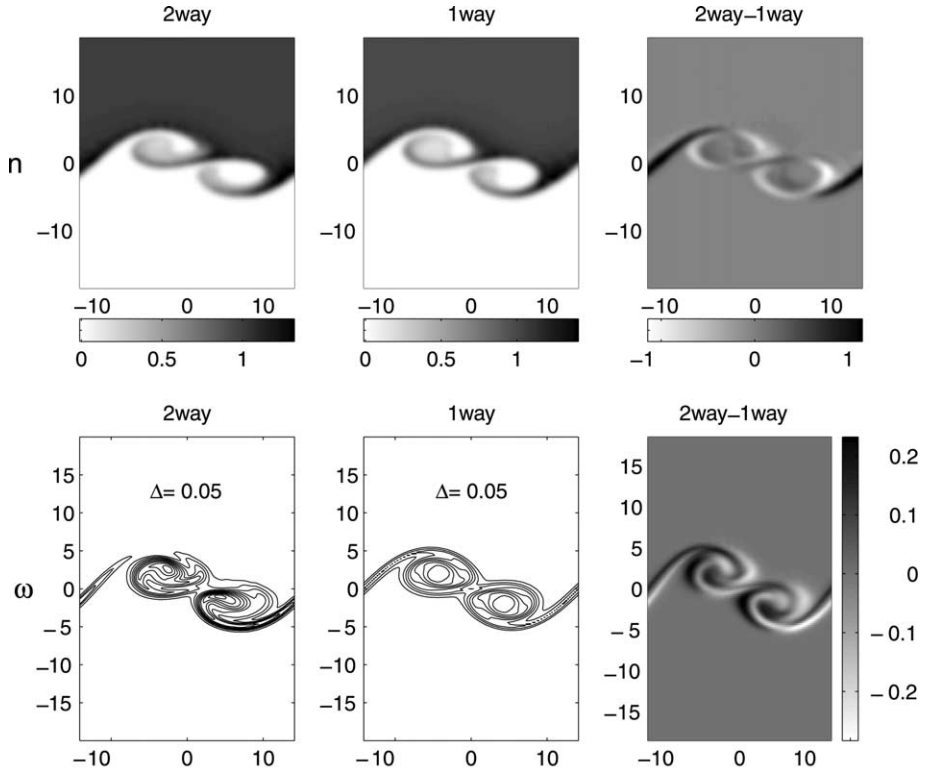

Fig. 7. $St = 0.1$, $D = 0.5$, $Re = 200$, $t = 37.5$, differentially seeded flow: Particle concentration and fluid vorticity fields for coupled and passive cases. The part of the braid immediately upstream of the vortex pair is weakened, while the braid section on the downstream side is strengthened.

the findings by Kiger and Lasheras (1995), whose normalized attenuation r.m.s. cross-stream profiles indicate substantially larger concentration peaks for the fundamentally forced case than for the subharmonic one. Equally important, for the subharmonically forced case the concentration peak is located substantially farther away from the centerline of the mixing layer than for the fundamental case. This is again in agreement with the measurements by Kiger and Lasheras (1995). Overall, our two-way coupled simulations thus confirm the observation by these authors that vortex pairing plays a homogenizing role on the particulate concentration field. A primary reason for this behavior can be seen in the fact that the strain field continuously changes its orientation with time as the vortices rotate around each other, so that over time it transports particles in different spatial directions.

4.2. Differential particle loading

Here the focus will be on the case where only one of the streams that make up the mixing layer is initially seeded with particles. This case was studied in detail experimentally by Kiger and Lasheras (1995, 1997). Again, the initial particle velocity is equal to the fluid velocity at the particle location. At the center of the mixing layer the flow field now contains a region of strong

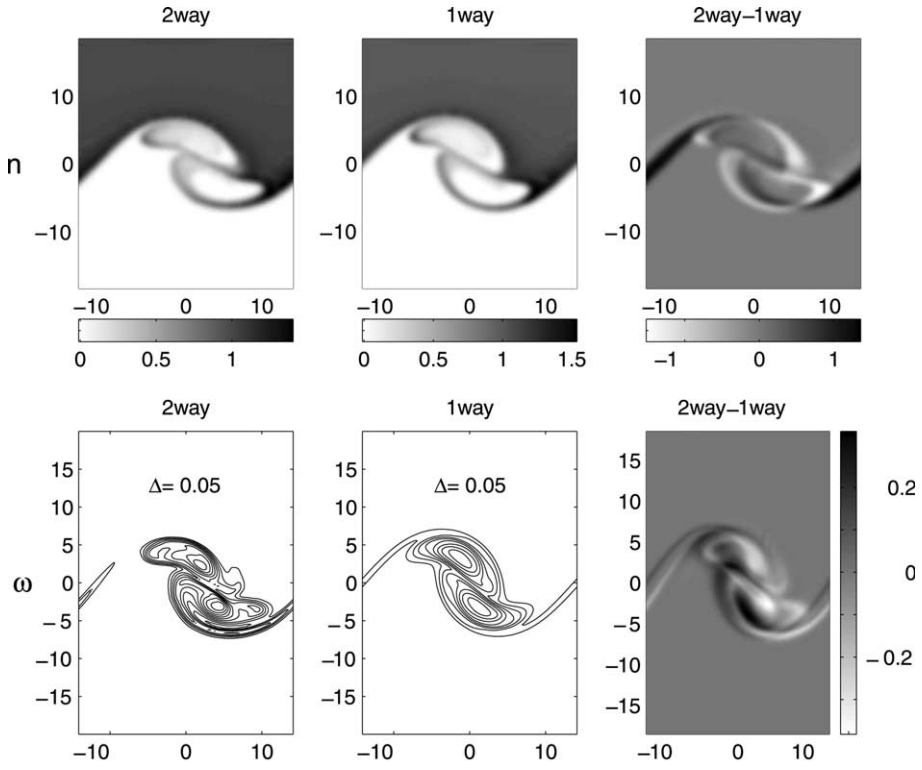

Fig. 8. $St = 0.1$, $D = 0.5$, $Re = 200$, $t = 50$, differentially seeded flow: Particle concentration and fluid vorticity fields for coupled and passive cases. The vortex pair is effectively displaced in the downstream direction.

particle number density gradient from the very beginning, so that according to Eq. (14) we expect to see an effect of the particulate phase on the fluid vorticity from the very start. This is in contrast to the uniformly seeded flow analyzed above, in which such gradients evolved only with time as particles accumulated in some regions, while being ejected from others.

During the initial phase, which is dominated by the growth and saturation of the fundamental perturbation, the evolution of the particle concentration and fluid vorticity fields displays several of the features that were already observed for the fundamental case (Meiburg et al., 2000). Specifically, for low Stokes numbers (Figs. 7 and 8) two high concentration particle streaks or tongues quickly emerge, one between the pairing vortices and one between the vortex pairs. As the subharmonic component grows in strength, however, clear differences with respect to the purely fundamental case emerge. In agreement with the experimental measurements of Kiger and Lasheras (1995), we find that soon the streak located between vortex pairs becomes more pronounced than the one between the pairing vortices. Due to the relatively weak temporal changes in the directionality of the strain field between vortex pairs, the high particle concentration band in this area retains its orientation over long times. The strain field in between the pairing vortices, on the other hand, continuously rotates throughout the vortex pairing process, which leads to a corresponding reorientation of the particle streak located there. It thus rotates with the pairing

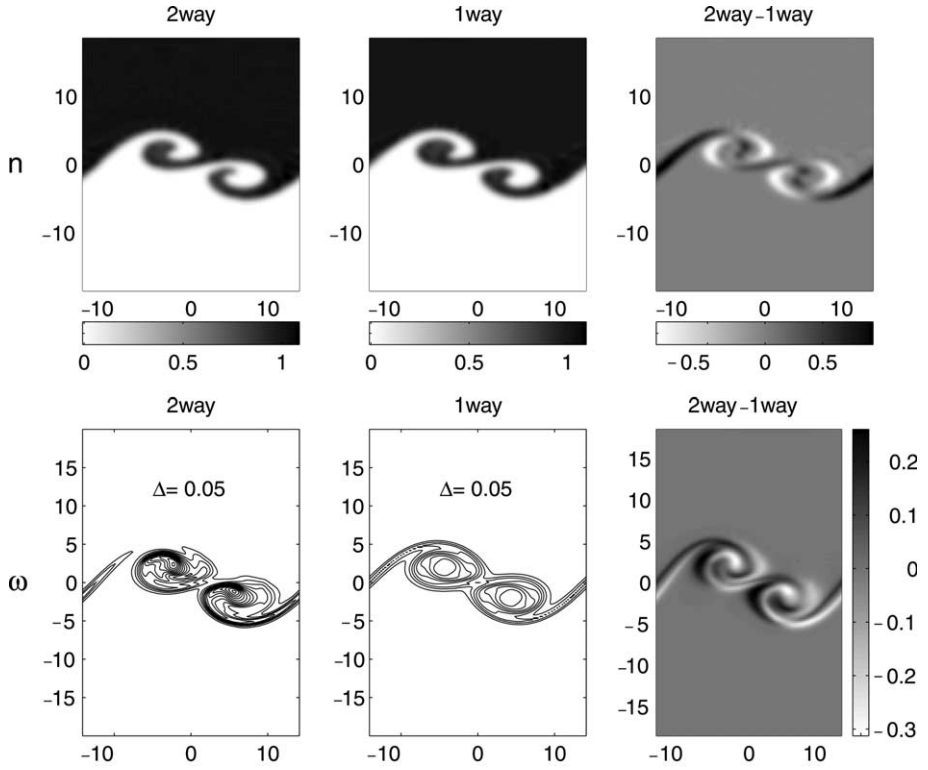

Fig. 9. $St = 1$, $D = 0.5$, $Re = 200$, $t = 37.5$, differentially seeded flow: Particle concentration and fluid vorticity fields for coupled and passive cases. The two-way coupling mechanisms affect the flow similarly to the $St = 0.1$ case.

vortices and eventually forms a closed loop. In the corresponding vorticity plot, we observe that the upstream (left) braid pinches off while the downstream (right) one gains in strength, which indicates a net downstream displacement of the concentrated vortices. This behavior is due to the concentration gradient term on the right-hand side of Eq. (14), which results in the cancellation of the local vorticity just upstream of the vortex pair, and in its amplification just downstream. Overall, this renders the upstream one of the pairing vortices weaker, while strengthening the downstream one, thereby introducing a certain asymmetry into the vortex pairing process. It is thus interesting to observe that, due to the concentration gradient term, the differentially loaded mixing layer can modify the base flow substantially even for small values of St. This had not been the case for the uniformly loaded case.

For intermediate Stokes numbers, a somewhat different picture emerges, cf. Figs. 9 and 10. The particles are now ejected more efficiently from the vortex cores. However, pronounced streaks are still seen to wrap around the cores. The asymmetry observed above persists, so that the upstream vortex is weakened, while the downstream one strengthens. As a result, the stronger vortex assumes a dominant role during the pairing process, and the weaker one wraps around it in an almost passive fashion. The asymmetry is reflected in the particle concentration pattern as well. By

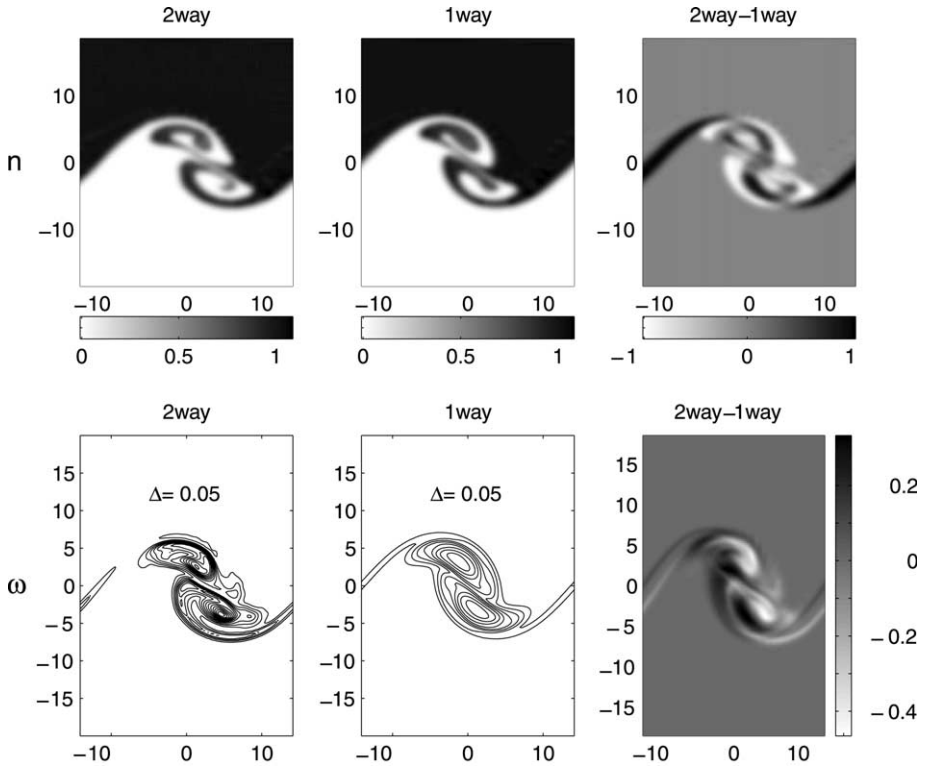

Fig. 10. $St = 1$, $D = 0.5$, $Re = 200$, $t = 50$, differentially seeded flow: Particle concentration and fluid vorticity fields for coupled and passive cases.

$t = 50$ the weaker, upstream vortex has ejected substantially fewer particles than the stronger, downstream one, whose core has become more or less entirely depleted of particles, cf. Fig. 10.

For higher values of St (cf. Figs. 11 and 12), the two particle bands can still be identified. However, due to the low particle responsiveness these bands do not wrap around the individual vortices or the emerging vortex pair in the same pronounced fashion as for lower St values. While the asymmetric evolution of the two vortices persists, the braid vorticity layer between vortex pairs thickens as a result of the increased damping of the mixing layer instability by the particles. By $t = 50$, this thicker braid has begun to roll up and to form an additional smaller 'satellite' vortex structure.

Fig. 13 depicts the two-way coupled flow fields for all three St-values at the late time $t = 62.5$. All three cases clearly display the above asymmetry by which the fundamental vortex originally located upstream has been weakened, while the downstream one has emerged stronger. The concentration fields for $St = 0.1$ and 1 still somewhat reflect the shape of the underlying vorticity field, while for $St = 10$ the particles have preferentially accumulated in the braids between the vortex pairs. This observation again is in agreement with the experimental findings of Kiger and Lasheras (1995), who note that the pairing process affects particles of different sizes in very different ways. In particular, they find that the resulting concentration field is less homogeneous for larger particles, which is confirmed by Fig. 13.

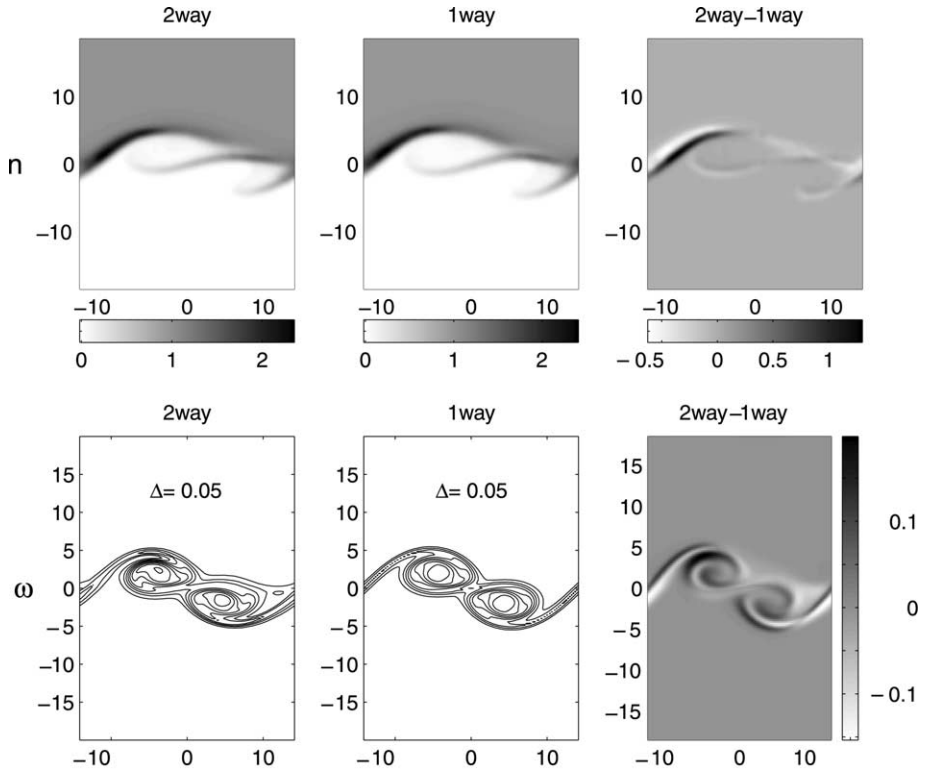

Fig. 11. $St = 10$, $D = 0.5$, $Re = 200$, $t = 37.5$, differentially seeded flow: Particle concentration and fluid vorticity fields for coupled and passive cases.

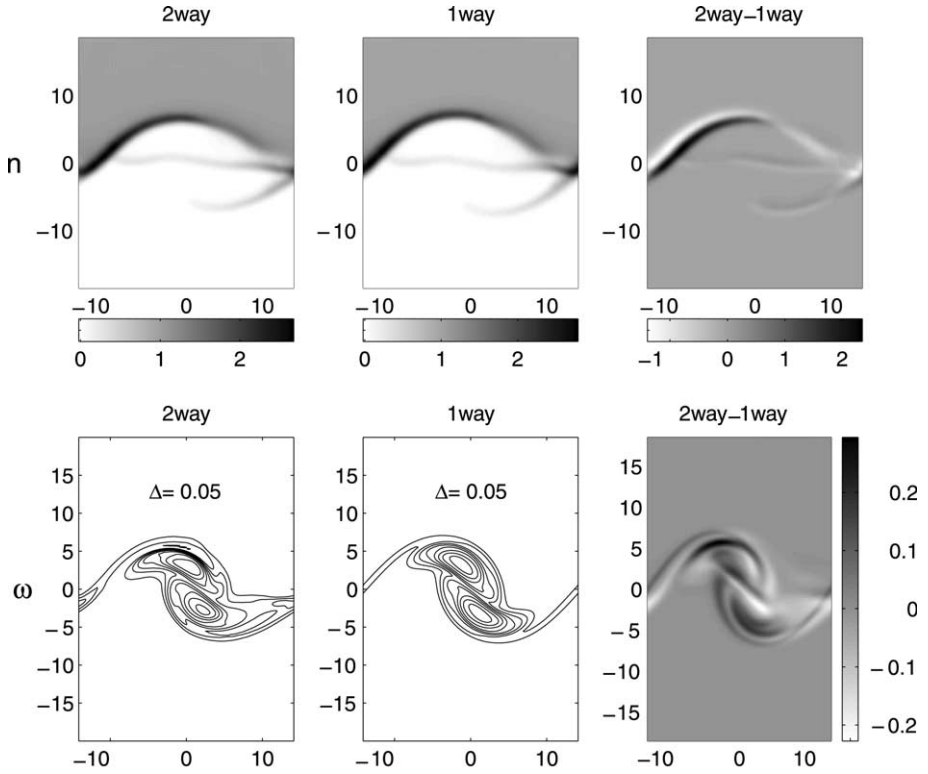

Fig. 12. $St = 10$, $D = 0.5$, $Re = 200$, $t = 37.5$, differentially seeded flow: Particle concentration and fluid vorticity fields for coupled and passive cases. At these large St values, the high-concentration particle bands no longer rotate with the pairing vortices, as had been the case for lower St.

For the differentially seeded flow, a suitable weighted particle displacement thickness is defined as

$$\delta(t) = \frac{1}{L} \int_{-L/2}^{L/2} \int_{-\infty}^{0} |y| n(y,t)\, \mathrm{d}y\, \mathrm{d}x. \tag{16}$$

It is striking that, inspite of the clearly identifiable local effects discussed above, coupling does not seem to have a strong influence on this streamwise averaged, quantitative measure of dispersion, independent of St, cf. Fig. 14. This appears to indicate that, in an integral sense, the growth of the subharmonic perturbation remains largely unaffected by the two-way coupling effects for a differentially seeded mixing layer. It is particularly noteworthy that the $St = 0.1$ particles exhibit the strongest overall dispersion. Considering the many claims in the literature of 'optimal' dispersion for intermediate St values, this may be somewhat surprising. However, it is in agreement with the passive simulations of Martin and Meiburg (1994), as well as with the experimental measurements of Kiger and Lasheras (1995). These authors point out that for small isolated regions of space and time, particles of intermediate St values can display optimal dispersion, while the integral dispersion measure that accounts for particles coming from all regions of the flow shows a maximum for passive tracer particles.

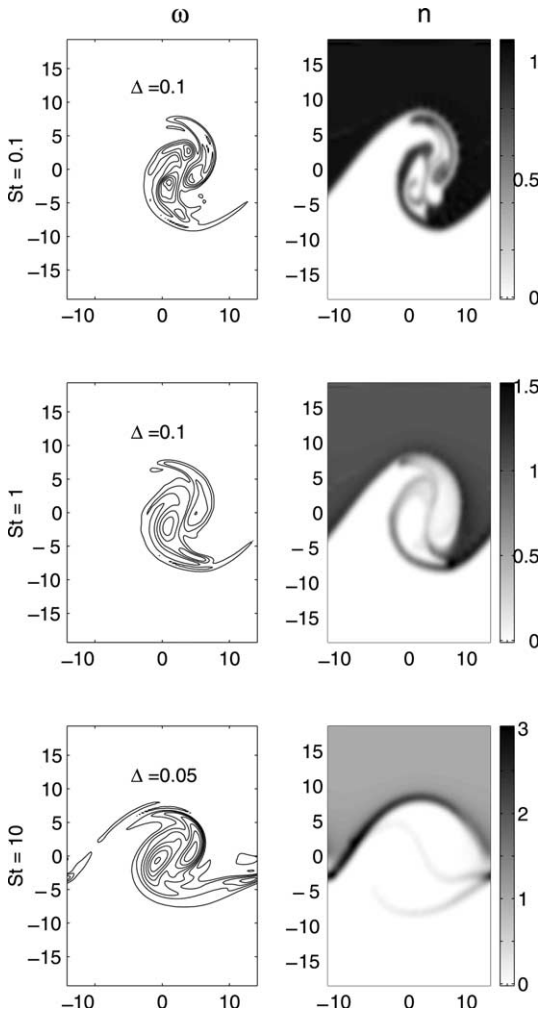

Fig. 13. $D = 0.5$, $Re = 200$, $t = 62.5$, $St = 0.1$, 1, and 10: In all three cases, the vortex originally located upstream has substantially weakened. The largest St particles have experienced the strongest ejection from the vortex pair.

5. Summary and conclusions

The present investigation aims at further elucidating the role of two-way interphase coupling effects, with emphasis on subharmonically forced, dilute particle laden mixing layers exhibiting forcing, by means of two-dimensional temporally growing computational simulations. The goal is to arrive at a vorticity-based interpretation of the numerical observations. By rewriting the source term that arises in the fluid vorticity equation as a result of the two-way coupling effects, we were able to show that particle concentration gradients can locally cancel or amplify the fluid vorticity field, whereas the 'slip vorticity' of the particles will usually dampen the fluid vorticity. Especially the first term is expected to lead to very different effects in uniformly and differentially loaded mixing layers, respectively. This in indeed confirmed by the simulations presented above.

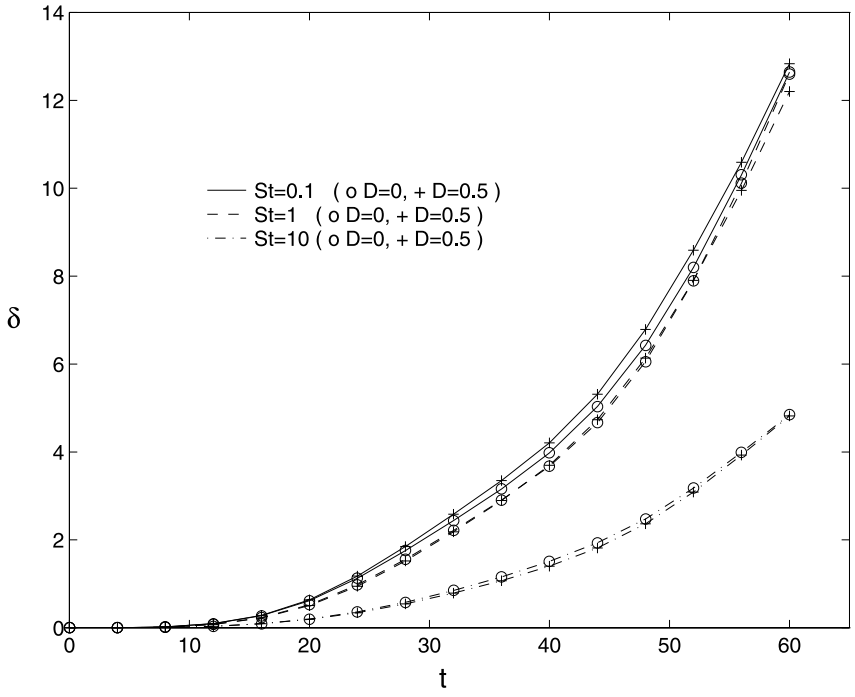

Fig. 14. Influence of *St* and two-way coupling on the weighted particle dispersion thickness for subharmonically perturbed, differentially seeded flow. The effect of the two-way coupling mechanisms is much less pronounced than for the uniformly seeded counterparts.

For uniformly laden mixing layers, intermediate *St* particles are seen to reduce the growth rate of the Kelvin–Helmholtz instability by delaying the vorticity transport from the braids into the vortex cores. As a result, the subharmonic vortex pairing process, which feeds on the fundamental instability, is slowed down as well. During the growth of the pairing process the braid in between the pairing vortices thickens, and it is depleted of particles much more rapidly than the braid in between the vortex pairs. Large *St* particles are seen to affect the mixing layer somewhat differently. The braids are now thicker, and due to the increased particle inertia they can even contain two bands of high particle concentrations. These, in turn, through the action of the vorticity source term, lead to a layered structure of the vorticity field in the outer regions of the core.

In the presence of a subharmonic perturbation, dispersion is not only a result of particle ejection from the vortex cores, but also of the particle transport *with* the vortex cores into the outer regions of the mixing layer, during the pairing process. Intermediate *St* particles are seen to be able to benefit from this mechanism the most, so that they can at least temporarily exceed the dispersion rate of the passive mixing layer case. Overall, however, particle dispersion is seen to be reduced by the two-way coupling effects, due to the slowing of the Kelvin–Helmholtz and vortex pairing instability. In general, the subharmonic case is found to lead to a more homogenized streamwise averaged concentration profile as compared to the fundamental case, in agreement with the experimental measurements by Kiger and Lasheras (1995).

While for temporally growing mixing layers uniformly laden with particles the symmetry of the vortex pairing process is maintained throughout, this is not the case for differentially loaded mixing layers. The vorticity source term related to the particle number density gradient now has a strong influence from the very beginning. Specifically, it is seen to weaken the upstream partner in the vortex pairing process, while strengthening the downstream one, which thus comes to dominate the pairing event. This mechanism is clearly visible even for small *St* particles, whereas in the uniformly laden case such particles have a negligible influence on the flow. For intermediate *St* particles, the above asymmetry leads to a much more rapid ejection of particles from the downstream vortex, whereas the upstream vortex core retains particles up to substantially longer times. For large *St* particles, the braid region in between vortex pairs is seen to thicken and to roll up, thereby leading to the emergence of a satellite vortex structure. Overall, our simulations confirm the findings by Kiger and Lasheras (1995), in that the particle dispersion field is much more non-uniform for large *St* particles. Somewhat surprisingly perhaps, our results indicate that in a streamwise averaged sense the two-way coupling effects do not significantly alter the integral particle dispersion measure for subharmonically forced, differentially loaded mixing layers.

Acknowledgements

This research was partially funded by NASA's Marshall Space Flight Center, and the collaboration with Dr. Munir Sindir of Boeing as well as the PVAMU/Rocketdyne CFD Institute is gratefully acknowledged. E.W. thanks the Flughafen Frankfurt/Main Stiftung and the Dr. -Jürgen-Ulderup-Stiftung for financial support during his visit at the University of Southern California. The simulations were partially carried out at the San Diego Supercomputer Center, which is funded by the National Science Foundation.

References

Dimas, A.A., Kiger, K.T., 1998. Linear instability of a particle-laden mixing layer with a dynamic dispersed phase. Phys. Fluids 10, 2539–2557.

Druzhinin, O.A., 1995. On the two-way interaction in two-dimensional particle-laden flows: the accumulation of particles and flow modification. J. Fluid Mech. 297, 49–76.

Elghobashi, S., Truesdell, G.C., 1993. On the two-way interaction between homogeneous turbulence and dispersed solid particles. I: Turbulence modification. Phys. Fluids A 5, 1790–1801.

Fessler, J.R., Eaton, J.K., 1999. Turbulence modification by particles in a backward-facing step flow. J. Fluid Mech. 394, 97–117.

Gottlieb, D., Orszag, S.A., 1977. Numerical Analysis of Spectral Methods: Theory and Applications. SIAM, Philadelphia, PA.

Kiger, K.T., Lasheras, J.C., 1995. The effect of vortex pairing on particle dispersion and kinetic energy transfer in a two-phase turbulent shear layer. J. Fluid Mech. 302, 149–178.

Kiger, K.T., Lasheras, J.C., 1997. Dissipation due to particle/turbulence interaction in a two-phase, turbulent, shear layer. Phys. Fluids 9, 3005–3023.

Kulick, J.D., Fessler, J.R., Eaton, J.K., 1994. Particle response and turbulence modification in fully developed channel flow. J. Fluid Mech. 277, 109–134.

Lazaro, B.J., Lasheras, J.C., 1989. Particle dispersion in a turbulent, plane, free shear layer. Phys. Fluids A 1, 1035–1044.

Lele, S.K., 1992. Compact finite difference schemes with spectral-like resolution. J. Comput. Phys. 103, 16–42.
Martin, J.E., Meiburg, E., 1994. The accumulation and dispersion of heavy particles in forced two-dimensional mixing layers. I. The fundamental and subharmonic case. Phys. Fluids 6, 1116–1132.
Maxey, M.R., Patel, B.K., Chang, E.J., Wang, L.-P., 1997. Simulations of dispersed turbulent multiphase flow. Fluid Dyn. Res. 20, 143–156.
Maxey, M.R., Riley, J.J., 1983. Equation of motion for a small rigid sphere in a nonuniform flow. Phys. Fluids 26, 883–889.
Meiburg, E., Wallner, E., Pagella, A., Riaz, A., Härtel, C., Necker, F., 2000. Vorticity dynamics of dilute two-way-coupled particle-laden mixing layers. J. Fluid Mech. 421, 185.
Michalke, A., 1964. On the inviscid instability of the hyperbolic-tangent velocity profile. J. Fluid Mech. 19, 543–555.
Pan, Y., Banerjee, S., 1996. Numerical simulation of particle interactions with wall turbulence. Phys. Fluids 8, 2733–2755.
Squires, K.D., Eaton, J.K., 1990. Particle response and turbulence modification in isotropic turbulence. Phys. Fluids A 2, 1191–1203.
Sundaram, S., Collins, L., 1999. A numerical study of the modulation of isotropic turbulence by suspended particles. J. Fluid Mech. 379, 105–143.
Truesdell, G.C., Elghobashi, S., 1994. On the two-way interaction between homogeneous turbulence and dispersed solid particles. II: Particle dispersion. Phys. Fluids 6, 1405–1407.
Wallner, E., Meiburg, E., 1998. Numerical simulation of two-way coupled particle laden mixing layers. In: Proceedings of the Third International Workshop on Vortex Flows and Related Numerical Methods, Toulouse, France, August 24–27.
Williams, F.A., 1985. Combustion Theory, second ed. Benjamin/Cummings, Menlo Park, CA.
Winant, C.D., Browand, F.K., 1974. Vortex pairing: the mechanism of turbulent mixing layer growth at moderate Reynolds number. J. Fluid Mech. 22, 237–255.
Wray, A.A., 1991. Minimal storage time-advancement schemes for spectral methods (preprint).